Soft Matter
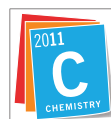
PAPER
Simon J. Haward *et al.*
Extensional opto-rheometry
with biofluids and ultra-dilute
polymer solutions

International Year of
CHEMISTRY
2011

2011
C
CHEMISTRY

RSCPublishing

1744-683X(2011)7:21;1-J

Extensional opto-rheometry with biofluids and ultra-dilute polymer solutions

Simon J. Haward,[*ab] **Vivek Sharma**[b] **and Jeffrey A. Odell**[a]

Complex fluids containing long polymer chains exhibit measurably large resistance to stretching or extensional flows, due to additional stresses generated by the extensional deformation of the underlying fluid microstructure. Understanding and quantifying the response of such elastic fluids to extensional flows is necessary for optimizing fluid composition for technological applications like ink-jet printing, spraying and turbulent drag reduction, as well as for fundamental understanding of polymer chain dynamics and refining constitutive equations. Using the opto-microfluidic technique of cross-slot extensional flow oscillatory rheometry (EFOR: J. A. Odell and S. P. Carrington, *Journal of Non-Newtonian Fluid Mechanics*, 2006, **137**, 110–120), we characterize the extensional response of ultra-dilute polymer solutions, hyaluronic acid (ubiquitous in the body: synovial fluid, vitreous body of eye) and saliva. Using microlitre sample volumes and piezo-pumps for fine control over shear and extension rates, we measure the additional stress in terms of enhanced pressure drop and intensity of birefringence that results from macromolecular deformation around the stagnation point created within the cross-slot geometry. We first show that the stress-optical coefficient obtained from the slope of the birefringence *vs.* pressure drop curve (stress optical curve) measured in the EFOR for dilute atactic-polystyrene (a-PS) in dioctyl-phthalate (DOP) solution, corresponds well to literature values. In the limit of ultra-dilute solutions where the excess pressure drop in extensional flow is negligible, we show that it is possible to quantify the extensional response using the birefringence from the stretched chains, allowing apparent extensional viscosity measurements from a-PS/DOP solutions with as little as 2 ppm of added polymer. We also use the flow birefringence measurements to perform "hydrodynamic chromatography" and are able to reconstruct the molecular weight distribution of the closely monodisperse a-PS sample. Additionally, we characterize the extensional viscosity response and present stress optical curves for hyaluronic acid (HA) solutions and saliva, also extracting the molecular weight distributions of these fluid samples using the a-PS as a calibration standard. We believe that measuring extensional properties of biofluids using low fluid volumes in the EFOR is promising for developing diagnostic methods and improving the performance of synthetic replacements for body fluids.

1. Introduction

Extensional flows that involve stretching of fluid elements arise in many natural and industrial processes, including inkjet printing, filament spinning, porous media flow, extrusion, moulding, coating, particle suspension/sedimentation, turbulent drag reduction, blood circulation, mucus flows (in *e.g.* lungs, eyes, mouth, *etc.*) and the flow of synovial fluid between joints under compression. The fluids used in most of these applications are termed complex fluids or viscoelastic materials as their response to applied stress (or strain) involves a combination of solid-like

elasticity and liquid-like ability to flow. For a fluid confined between two plates, the response to an applied stress (or strain) is measured typically using a torsional rheometer, where the shear viscosity describes the resistance offered by the fluid to a parallel displacement of the plates. In this case the velocity gradient is always perpendicular to the flow direction. If, on the other hand, the two plates are displaced so as to increase their separation, both flow and the velocity gradient are in the same direction resulting in a stretching or extensional flow field. Macromolecular stretching caused by the exposure of complex fluids containing long polymer molecules to extensional flow fields can lead to a much larger resistance to flow than expected on the basis of the shear viscosity measured in conventional torsional rheometers. While Trouton[1] showed that the uniaxial extensional viscosity of a Newtonian fluid is a factor of three times larger than shear viscosity, non-Newtonian (or complex) fluids can

---

[a]H. H. Wills Physics Laboratory, University of Bristol, Tyndall Avenue, Bristol, BS8 1TL, UK
[b]Massachusetts Institute of Technology, Department of Mechanical Engineering 77 Massachusetts Avenue, Cambridge, MA 02139, USA. E-mail: shaward@MIT.EDU; Tel: +1 6172530273

exhibit up to a thousand times higher extensional viscosity.[2–5] Empirically, it has been established that extremely low concentrations of high molecular weight polymers (parts-per-million) can exhibit remarkable non-Newtonian behaviour in extensional flows. Perhaps the most striking examples of this are the observation of turbulent drag reduction[6,7] and the dramatic increase in flow resistance observed in porous media flows.[8,9] In the biological world, the stringiness of saliva,[10] stickiness of carnivorous plants[11] and glue found on spider webs for catching insects[12] and fibre formation by spiders and silkworms,[13] are instances of macromolecules in physiological or biological fluids experiencing extensional flow fields. The characterization of the rheological response of biofluids presents a particular challenge as the sample volumes available are limited, and for physiological fluids like saliva, cervical mucus, synovial fluid and sputum where stringability can be used as a diagnostic tool, the ability to accurately characterize a small volume of fluid is necessary. Here we describe the quantitative measurement of the extensional response of ultra-dilute polymer solutions as well as low volumes of biofluids using a recently developed microfluidic device, the Extensional Flow Oscillatory Rheometer (EFOR).[14–18]

While fully developed flow within a channel or flow in cone-and-plate or Couette geometries on a torsional rheometer are simple shear flows,[19] extensional components arise in virtually all real fluid flows, in particular contraction/expansion flows,[20,21] bifurcations (i.e. 'T' or 'Y' junctions),[22] flow around obstacles[23] and stagnation points,[24] as well as in free surface flows such as spraying, jet break-up, drop formation and filament stretching.[25,26] Quantifying the extensional viscosity of fluids in any geometry or device remains one of the most challenging aspects of rheometry, due to the strong dependence on flow parameters including both the strain rate and the total available fluid strain.[27,28] In order for macromolecules to reach a high degree of extension in flow a dual condition must be satisfied. Firstly, the velocity gradient (or strain rate), $\dot{\varepsilon}$, must exceed the rate at which the macromolecule can relax, $1/\tau_{c-s}$, where τ_{c-s} is the longest relaxation time of the molecule in its coiled state; this is the *critical rate condition*. Secondly, the strain rate must be maintained for long enough for the required strain to accumulate in the molecule (flexible high molecular weight polymers can require strains of $100\times$ or more to become fully stretched); this is the *accumulated strain condition*. The dual rate and strain condition can be realized by incorporating a stagnation point in the flow field. A stagnation point is a singularity in a flow field where the flow velocity asymptotes towards zero but the strain rate can be large. Hence macromolecules that follow streamlines passing through the stagnation point become trapped in the velocity gradient for, in principle, infinite time and can accumulate significant strain provided $\dot{\varepsilon} > 1/\tau_{c-s}$.

Theoretical considerations by De Gennes[29] and Hinch[30] showed that for dilute solutions of highly coiled flexible macromolecules, strong hydrodynamic interactions (HI's) between chain segments meant that $\tau_{c-s} \equiv \tau_Z$, where τ_Z is the Zimm relaxation time.[31] In a strong extensional flow field, such that $\dot{\varepsilon} > 1/\tau_Z$, macromolecular stretching could be a critical, runaway process in which molecules approached full extension; termed the coil-stretch transition. The criticality is because of the change in HI's between chain segments as the coil unravels. In the highly coiled state many chain segments in the interior of the

coil are "screened" from the flow field by exterior segments. In this state the coil is termed "non-free draining", HI's are important and the chain obeys Zimm-like dynamics, $\tau_Z \propto M^{3/2}$, where M is the molecular weight.[31] As the coil unravels in the flow more chain segments become exposed to the solvent, HI's become less and less important and the chain becomes more "free-draining". In the unravelled, free-draining state the chain obeys Rouse-like dynamics such that $\tau_R \propto M^2$.[32] The expected increase in relaxation time between the coiled and stretched states led to the prediction of hysteresis in the coil–stretch–coil cycle with strain rate. Additionally, the coil–stretch transition would be accompanied by a huge increase in the extensional viscosity.[33]

Stagnation point flows can be generated in microfluidic devices such as T-junctions,[22,34] four-roll mill analogues[35–38] and cross-slots,[15,17,39–41] where small length scale and low flow rate reduce inertial contributions to the flow. Cross-slots consist of bisecting channels with opposing inlets and outlets, which form a stagnation point at the symmetry axis. Along the outflowing symmetry plane, within the central cross-over region, the cross-slots produce a good approximation to a pure planar extensional flow field.[42] High degrees of chain stretching at the stagnation point, and coil-stretch hysteresis have been demonstrated by studies of flow induced birefringence[14–16] and by direct observation of fluorescently labelled DNA[43–45] in cross-slot flow experiments. This stretching has also been shown to coincide with a significant increase in the pressure drop measured across the cross-slot, consistent with the predicted increase in the extensional viscosity.[14–16] Traditionally, cross-slot based-rheometers were designed as continuous flow devices, requiring a large volume of test fluid, O (1 ml) for a typical experiment. This has precluded their use to study many exotic or scarce fluids, such as most biological specimens. By using an oscillatory flow generated by piezo-driven micropumps to keep a small discrete volume of fluid trapped within a microscale cross-slot, the EFOR can make measurements using test fluid volumes as low as O (1 µL). The fluid microstructure is studied using flow-induced birefringence, which provides an indication of macromolecular strain.[46] Micro-particle image velocimetry (µ-PIV) can be used to quantify flow kinematics. Extensional rheometry, or viscometry, is typically accomplished by measurement of the pressure drop across an inlet and an outlet channel (see discussion later). Additionally, shear contributions to the measured pressure drop can be quantified to first order by direct measurement in the device, simply by shutting off two of the channels. The use of an oscillatory flow, combined with the reduction of the cross-slot dimensions down to the microscale and sensitive optics, has resulted in an extensional rheometer capable of measurements of relaxation times and extensional viscosities of polymer solutions of 'ultra-dilute' concentration, using small discrete amounts of fluid. Additionally, fluid within the cross-slot is enclosed in a clean and inert environment, ideal for biological samples, evaporation of volatile solvents is negligible and temperature control can be implemented relatively simply.

In this contribution, we infer the extensional response of a variety of non-Newtonian fluids using the EFOR technique. The piezo-driven cross-slot flow offers novel and unmatched advantages for studying extensional response. We first show that the simultaneous determination of pressure drop and birefringence in the EFOR provides us with a method for determining

the stress optical coefficient for dilute solutions using small sample volumes. The stress-optical coefficient is first determined for a thermodynamically ideal, model dilute solution of a monodisperse high molecular weight atactic-polystyrene (a-PS) in dioctyl phthalate (DOP), and the measured value matches values published in the literature. Using the stress-optical coefficient and measured birefringence, we can estimate the extensional stress as a function of nominal extensional rate for extremely dilute samples. The apparent extensional viscosity of ultra-dilute model polymer solutions (2 ppm or 0.0002 wt % $M_p = 10.2 \times 10^6$ g mol^{-1} a-PS in DOP) is measured by using birefringence from stretched polymer chains confined to the stagnation point. Similar concentrations are often encountered in drag reduction applications,[7] and the measurement of the extensional viscosity of polymer solutions with such high dilutions has been a long-standing challenge. Subsequently, the apparatus is used to study the extensional behaviour of a solution of hyaluronic acid, a high molecular weight polysaccharide used in eye drops and consumer care products and which is also the main functional component in synovial fluid. Finally, a real physiological non-Newtonian fluid, human saliva, is tested. Saliva is an example of a highly complex aqueous biofluid containing high molecular weight mucins and other proteins. We determine the stress-optical coefficient and the apparent extensional viscosity for both HA and saliva, highlighting the possibility of using opto-microfluidics methods incorporated in EFOR for diagnostics and for designing synthetic biofluids.

2. Material and methods

Ultra-dilute model polymer solution

The atactic polystyrene (a-PS) sample used in this study had a molecular weight of $M_p = 10.2 \times 10^6$ g mol^{-1} and was a gel permeation chromatography (GPC) calibration standard obtained from Polymer Laboratories Ltd. The sample was closely monodisperse with nominal $M_w/M_n = 1.17$. Dioctyl phthalate (DOP) is a viscous ($\eta_S = 0.046$ Pa s), thermodynamically ideal (θ), solvent for a-PS at close to room temperature.[47] Solutions of a-PS in DOP were prepared at concentrations 0.0002 wt.% $\leq c \leq 0.03$ wt.% using an intermediate solvent method. The overlap concentration, c^*, can be estimated based on simple cubic packing of polymer coils[48] using $c^* = (M_p \times 10^{-4})/N_A.(2R_g)^3 \sim 0.2$ wt.%, where N_A is Avogadro's constant and R_g is the radius of gyration of the equilibrium coil. The radius of gyration can be calculated using $6R_g^2 = C_\infty n\ell^2$, where $C_\infty = 9.7$,[49] $n = M_p/M_0$ is the number of monomers per molecule and $\ell = 0.25$ nm is the length of a monomer,[50] giving $R_g = 99.7$ nm. Hence, the a-PS/DOP solutions are in the range $c/c^* < \sim O(0.01)$ and can thus be considered 'ultra-dilute'.[51] In addition, it has been shown previously that for $c \leq 0.005$ wt.% this polymer/solvent system does not cause significant modifications to the Newtonian flow field when polymer chains are highly stretched out near the stagnation point, which could justly be considered the true criterion on which polymer solutions should be considered ultra-dilute.[15,51,52] The longest characteristic time of the polymer in the coiled state can be calculated using Zimm theory[31] to be $\tau_Z = 0.2\eta_S R_g^3/k_B T = 2.24$ ms, where k_B and T are the Boltzmann constant and the temperature, respectively. The $M_p = 10.2 \times 10^6$ g mol^{-1} a-PS macromolecule is

highly flexible under theta-solvent conditions with a contour length, $L = n\ell \sim 24.5$ μm and a persistence length, $p = C_\infty\ell/2 \sim 1.2$ nm, giving $\sim 20,000$ effective units of persistence length per molecule.

Biofluids

Hyaluronic acid solution. HA is a naturally occurring long-chain polysaccharide and the main functional polymeric component in synovial fluid. The rheological properties of synovial fluid, particularly in extension, are thought to be of vital importance in protecting the knee joint from sudden shock, *e.g.* from a high-load impacts such as occur during running or landing after a jump.[53] Degradation of the HA in synovial fluid is an aggravating symptom of osteoarthritis (OA) since the synovial fluid loses its protective properties, causing frictional contact between cartilage and bone as the disease progresses. Currently, clinical assessment of synovial fluid viscosity is performed simply by eye or by finger stretch.[54] The EFOR has the potential to perform detailed rheological testing of biopsy-sized synovial fluid samples, offering the possibility of comparing healthy and diseased fluid. Increased understanding of the changes in synovial fluid rheology due to disease could lead to significant improvement in prosthetic fluid formulation and therapies for OA patients, and potentially to a minimally invasive diagnostic tool.

A sample of high molecular weight (nominal $M_w = 3$–4×10^6 g mol^{-1}) linear hyaluronic acid (HA), obtained from cockerel comb, was procured from Sigma-Aldrich. The HA was dissolved to a concentration of 0.1 wt.% in a 0.01 M phosphate-buffered saline (PBS), also purchased from Sigma-Aldrich (pH 7.4, 0.138 M NaCl, 0.0027 M KCl). HA exists as a polyelectrolyte macromolecule with negative charges along the backbone, and its conformation will therefore be affected by the solution pH and ionic strength.[55,56] These charges will be partially screened by positive ions in the buffer solution, resulting in a relatively coiled and extendable molecule under equilibrium (no flow) conditions,[57,58] although hydrogen bonding and the innate structure of HA act to stiffen the molecule.[59] Light scattering studies on HA of similar M_w and under similar solvent conditions indicate an average radius of gyration of $R_g \sim 0.2$ μm and a corresponding equilibrium end-to-end length of $\langle r_0^2 \rangle^{1/2} = \sqrt{6}R_g \sim 0.5$ μm.[60,61] The contour length of the macromolecule can be estimated from the mass (400 g mol^{-1}) and the length (0.95 nm) of the D-glucuronic acid and N-acetyl-D-glucosamine dimer repeat unit,[62] giving ~ 7 μm $< L < \sim 10$ μm. The persistence length of HA has been reported to be $p \sim 7$ nm,[61] giving ~ 1000–1500 persistence lengths per macromolecule, hence we consider HA in PBS as a semi-flexible chain. This is in reasonable agreement with rheological measurements on HA in PBS, which obtained concentration scalings of the viscosity consistent with flexible, neutral polymers in good solvents.[63] The value of $R_g \sim 0.2$ μm provides an overlap concentration for HA in PBS of ~ 0.01 wt.%, indicating that the 0.1 wt.% test fluid is in the semi-dilute regime.

Saliva. Saliva is a mucous secretion that coats the surface of the oral cavity and is an aqueous mixture of high molecular weight (MUC5B) mucins (2×10^6 g mol^{-1} $< M_w < 40 \times 10^6$ g mol^{-1}),[64] lipids and other proteins and bioactive molecules.[65] The total mucin content in fresh saliva is thought to be around

0.02 wt.%.[66] Mucins are very high molecular weight glyco-conjugates consisting of a polypeptide backbone decorated by oligosaccharide side chains. Like HA, mucins are poly-electrolytes and carry negative charges under physiological conditions.[56] The dense glycosylation and repulsive charge interactions between chain segments favour extension of the macromolecule into a rod-like conformation.[56] The contour length of MUC5B mucin can be estimated as a function of molecular weight using the known protein fraction ($\sim$20%[67]) and the average mass and length of an amino acid (135 g mol^{-1} and 0.38 nm, respectively), giving $\sim$1 μm < L < $\sim$20 μm. Using an estimate of the persistence length of $p \sim$ 40 nm,[68] the radius of gyration can be obtained from the equilibrium end-to-end length, $\langle r_0^2 \rangle^{1/2} = \sqrt{2pL}$ using the wormlike chain model,[69] giving $\sim$0.1 μm < R_g < $\sim$0.5 μm, depending on M_w. Corresponding estimates of the overlap concentration indicate that the MUC5B in saliva exists slightly above c^*.[18] The rheology of saliva is important for numerous functions in the oral cavity such as mastication, bolus formation and swallowing.[70] Full characterization of the rheology of saliva in shear and extensional flows could help the formulation of accurate replacement fluids and treatments for conditions such as oral mucositis and Sjögren's syndrome.[71] Sjögren's syndrome is an autoimmune disease that results in the destruction of the exocrine glands which produce tears and saliva. Other conditions associated with the drastically altered rheology of mucus include cystic fibrosis, chronic obstructive pulmonary disease and acute asthma.[72,73]

Human whole saliva was collected by expectoration at approximately 9:00 am, between one and two hours after adequate oral hygiene, but before any food or drink had been consumed and without any form of artificial stimulation. Following collection the saliva was immediately centrifuged at 10,000 g (where g is the acceleration due to gravity) for 5 min in order to remove particulate matter, cells and bacteria that could interfere with the detection of birefringence and potentially block the microchannel. Following centrifugation, saliva samples were immediately tested in the EFOR. The effect of the centrifugation on the saliva rheological properties has been assessed in a previous publication.[18]

EFOR: Principle and apparatus

Cross-slot channels used in the work were cut through stainless steel by wire electrical discharge machining (wire-EDM) with a 100 μm diameter wire and were enclosed between soda-glass viewing windows. Wire-EDM results in highly parallel channel walls and smooth surface finish (see Fig. 1a,b), which are features vital to produce a stable and symmetric flow field. As opposed to soft photolithography, which is the standard method of producing microfluidic chips in poly(dimethyl siloxane) (PDMS), wire-EDM allows fabrication of slots with an almost unlimited aspect ratio. The slots shown in Fig. 1 have a channel width of $w = 200$ μm, depth of $d = 1$ mm (aspect ratio of 5 : 1) and length $l = 1.2$ mm. The high aspect ratio provides a long optical path length through the enclosed fluid (and hence enhanced birefringent signal) and also provides a quasi-2D flow. Additionally, as the slots are made with stainless steel and have glass windows, organic solvents can be used. The choice of solvents is limited in a PDMS flow cell as organic solvents can swell the polymer.
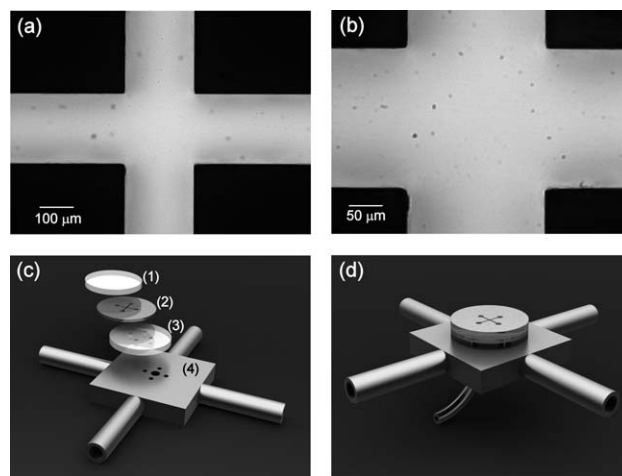

Fig. 1 (a) and (b) micrographs of the 200 μm wide cross-slots, which were fabricated by wire electrical discharge machining (wire-EDM). (c) Blown-up illustration of the construction of the cross-slot flow cell: (1) glass front window, (2) stainless steel cross-slot, (3) glass rear window and (4) stainless steel back plate with connections to 6 mm Swagelok tube fitting. (d) Illustration of cross-slot assembled with silicone adhesive, showing detail of the additional pipe to the rear of the back plate used for injection of exotic fluids.

The cross-slots were assembled as shown schematically in Fig. 1c,d. The soda glass front and rear windows were annealed at 300 °C for 24 h to remove residual stresses. All components were bonded together using a silicone adhesive. The backplate (4) in Fig. 1c has four connections to the main flow system of pumps and pressure sensor (described below) plus an additional pipe to the rear used for the injection of exotic or scarce fluids (see detail in Fig. 1d). This allows test fluid to be injected only into the cross, while the rest of the apparatus (i.e. pumps and pipes) is filled with a solvent used as a hydraulic fluid to drive the flow. Tests have shown that mixing between the test fluid and surrounding solvent is slow compared with the time scale of an experiment, which typically takes <5 s.[18]

The cross-slots are incorporated into the EFOR system as illustrated schematically in Fig. 2. The piezoelectric micro-pumps (1) are driven by applying oscillating triangular voltage profiles
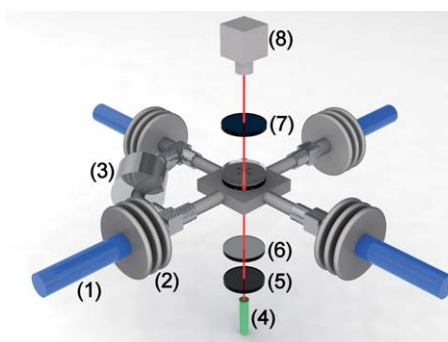

Fig. 2 Schematic illustration of flow system and optical line for birefringence measurements in the cross-slots, showing (1) piezo stacks, (2) stainless steel bellows, (3) Druck differential pressure sensor, (4) solid state laser, (5) polarizer, (6) λ/4 plate, (7) analyser and (8) Andor cooled CCD camera.

(corrected for piezo hysteresis) of amplitude $V/2$ and period T across them. The piezos extend/contract by $\sim$1 μm per applied volt. This results in a linear compression/expansion of each bellows (2) and hence a constant volume flow rate $Q \approx (2a_{eff}V)/T$ through each channel of the slot, where $a_{eff} \approx 4 \times 10^8$ μm^2 is the effective cross-sectional area of the bellows.

The superficial flow velocity, U, in each channel is given by:

$$U = \frac{Q}{wd}. \quad (1)$$

The nominal strain rate at the stagnation point, $\dot{\varepsilon}$, is given by:

$$\dot{\varepsilon} = \frac{2U}{w}. \quad (2)$$

$\dot{\varepsilon}$ is defined on the assumption that fluid accelerates linearly from zero velocity at the stagnation point at the centre of the cross up to the superficial flow velocity, U, at the start of the exit channel of the cross, a distance $w/2$ away. This provides a good approximation for the average strain rate between the channel entrances for the flow of Newtonian fluids and low concentration polymer solutions which do not significantly modify the flow field when they stretch.[15]

Viscoelastic effects within the flow geometry can be characterized by Deborah number, that compares the relaxation time of the fluid to the relevant experimental time scale. The Deborah number, De, of the flow is given by the ratio of polymer stretching characteristic time, τ_{c-s}, to characteristic flow time, $1/\dot{\varepsilon}$:

$$De = \dot{\varepsilon} \cdot \tau_{c-s}. \quad (3)$$

There has been recent discussion in the literature questioning the use of eqn (3) to define the Deborah number.[74] However we have chosen to retain the notation to maintain consistent nomenclature with related publications (e.g. ref. 14,15,43,44) using cross-slot geometries.

Inertial contributions to the flow are characterized by the Reynolds number, Re, defined by:

$$Re = \frac{\rho U D_h}{\eta} \quad (4)$$

where ρ is the solvent density, η is the fluid viscosity and D_h is the hydraulic diameter, given by $D_h = 2wd/(w + d)$.

In principle the piezos could be driven at a maximum of $V = 100$ volts and a frequency of 100 Hz ($T = 0.01$ s), which corresponds to $Q \sim 8$ mL s^{-1} and $\dot{\varepsilon} \sim 400{,}000$ s^{-1}. In practice the lower bound on T can be limited by the rise time (Δt) for the pressure drop to reach a quasi-steady state, which for Newtonian solvents is $\sim$50–100 ms. Therefore the minimum value of T is $\sim$ 0.5 s and the maximum attainable strain rate is $\dot{\varepsilon} \sim 8{,}000$ s^{-1}. Generally it is desirable to reach a steady flow before making measurements (all the data presented in this article were collected under quasi-steady state flow conditions). The maximum value of Q is also limited by the Reynolds number (Re), which it is desirable to maintain as low as possible to minimize inertial effects (we have found anomalous increases in the excess pressure drop for $Re > \sim$50). The lower limit on pumped volume is set by the bit size of the digital output to the piezo actuators. This corresponds to a minimum piezo step displacement of $\sim$25 nm ($\sim$0.025 V applied) and a volume pulse of $\sim$10 nL. However, it is desirable to have a non-pulsatile flow and

the practical lower limit on volume flow rate was found for $\sim$40 pulses ($V = 1$ V) applied over a time $T/2 = 2.5$ s. This corresponds to $Q \sim 0.16$ μL s^{-1} and $\dot{\varepsilon} \sim 8$ s^{-1}.

The piezos can also be used to draw an accurate volume of test fluid from a syringe positioned at the injection point depicted in Fig. 1d. For example, if a test is to be performed at an operating voltage of $V = 10$ V, then all four piezos can be extended by 10 V ($\sim$10 μm). Appropriate valves can be opened/closed such that, when the piezos are retracted back to the 0 V position, the required volume of test fluid is loaded into the cross-slot. For $V = 10$ V this volume is $\sim$4 μL per pump (16 μL in total) and the practical range of available strain rates is $\sim$80 s$^{-1} \leq \dot{\varepsilon} \leq \sim$800 s^{-1}, depending on the choice of T.

All of the constraints outlined above can be adjusted to a certain extent by e.g. using bellows of different a_{eff} or piezos with a different displacement range. However, the single largest difference can be achieved by altering the channel width, w, of the cross-slots. Since the volume of fluid required to fill the channel is proportional to w and, for a given Q, $\dot{\varepsilon} \propto 1/w^2$ and $Re \propto w^2$ it is clear that, by reducing w, considerable advantages can be obtained in terms of required fluid volumes, maximum available strain rates and minimising inertia. The disadvantage is an increase in the lower limit on $\dot{\varepsilon}$; this could be overcome by greater bit depth on the digital-analogue converter. It is possible to perform wire-EDM with a 30 μm diameter copper wire, allowing production of slots with $w \sim 50$ μm and essentially any required value of d.

The pressure difference in the cross-slots is measured across an inlet and an outlet channel using a Druck differential pressure sensor (3) shown schematically in Fig. 2. By disconnecting two of the pumps and simply measuring the pressure drop for flow of fluid around a corner of the cross-slot (ΔP_{shear}) a measure of the shear viscosity, η_{shear}, can be obtained. Assuming Poiseuille flow in a rectangular channel of total length $2l$ and neglecting the small perturbation resulting from the presence of the corner of the cross:[75]

$$\eta_{shear} \approx \frac{w^2 \Delta P_{shear}}{24Ul}. \quad (5)$$

However, although eqn (5) gives a good approximation to the shear viscosity,[16] η_{shear} can be determined more reliably using conventional rheological methods. The main reason for measuring ΔP_{shear} in the cross-slots is so that it can be subtracted from the pressure drop measured with all four pumps running (ΔP_{total}) in order to obtain the excess pressure drop (ΔP_{excess}) due to the extensional component in the flow-field. Assuming $\Delta P_{excess} \propto \sigma_{ext}$, where σ_{ext} is the extensional stress in the stretching fluid, we can obtain a measure of the extensional viscosity of the fluid thus:

$$\eta_{ext} \propto \frac{\Delta P_{excess}}{\dot{\varepsilon}} = \frac{\Delta P_{total} - \Delta P_{shear}}{\dot{\varepsilon}}. \quad (6)$$

The optics used for birefringence observation and measurement are also shown in Fig. 2. The light source (4) was a stabilized 660 nm 60 mW fibre-coupled diode laser from Oz Optics. The polarizer (5) and analyzer (7) were crossed at $\pm$ 45° to the direction of the channels of the cross-slot and a quarter-wave plate (6) was used to compensate for residual birefringence in the system to achieve the maximum possible extinction. The CCD

camera from Andor Technology (8) was a deeply cooled ($-80\,°C$), very low noise, high quantum efficiency ($\sim60\%$), 14 bit, 1000×1000 pixel camera capable of frame rates up to several hundred per second. A stable, low noise imaging system and polarizers with very high extinction ratio are essential for detection of the low birefringence signals obtained from dilute polymer solutions.

3. Results and discussion

Ultra-dilute model a-PS/DOP solutions

The zero shear viscosity of dilute polymer solutions increases linearly with polymer concentration, and the concentration dependence can be described with an equation analogous to Einstein's equation for viscosity of suspensions, assuming that coil–coil interactions are negligible.[76] With increasing concentration, coils begin to overlap at a number density at which a single polymer coil is present in every unit volume, and this concentration is termed as the overlap concentration.[76] The overlap concentration for the $M_p = 10.2 \times 10^6$ g mol^{-1} a-PS molecule in DOP can be estimated using well-established molecular parameters to be $c^* \sim 0.2$ wt.%. In the experiments described herein, the solution concentrations are as low as 0.0002 wt.% (or $c^*/1000$), implying that they are ultra-dilute solutions.

A control volume of the polymer solution is inserted into the cross-slot and the molecular stretching of the chains close to the stagnation point is characterized by measuring the birefringence response from the channel, while pressure drop required to sustain a chosen flow rate is measured as well. The dilute solution response is presented and discussed first as a base case, before proceeding to the response from polymer solutions with extreme dilution. The birefringence data obtained from a 0.03 wt.% solution ($c/c^* = 0.15$) of a-PS in DOP at a strain rate of $\dot{\varepsilon} = 1025$ s^{-1} under the influence of oscillatory flow driven by the piezo micropumps is shown in Fig. 3 where schematics alongside describe the piezo micropump motion. The dilute solution response in Fig. 3a demonstrates the observed birefringent elastic strand for outflow along the horizontal axis, while Fig. 3b shows what happens when the flow reverses direction. Fig. 3c shows how the measured pressure drop ΔP_{total} for the same polymer solution varies when the flow switches direction. For this polymer solution a time of $\Delta t \sim 250$ ms was required for the pressure drop to reach steady state. The relatively long Δt (compared with Newtonian fluid) is likely due to a progressive modification of the flow field due to the increasing extensional viscosity as the polymer molecules stretch and become birefringent.[15] The measured birefringence and excess pressure drop ($\Delta P_{excess} = \Delta P_{total} - \Delta P_{shear}$) as a function of nominal extension rate (eqn (2)) are shown in Fig. 3d. The stress-optical diagram plotted in the inset of Fig. 3d shows the trace of optical birefringence against the measured pressure drop. The birefringence from macromolecular stretching is linearly proportional to the excess pressure drop measured, in other words the fluid appears to obey the stress-optical rule (SOR), $\sigma_{ext} = \Delta n/C$, where σ_{ext} is the stress and C is the stress-optical coefficient. The slope of the stress-optical diagram provides the value for stress-optical coefficient to be $C = -5.7 \times 10^{-9}$ Pa^{-1}. The measured value agrees very well with the values reported in the literature, which range between -4×10^{-9} Pa$^{-1} < C < -6 \times 10^{-9}$

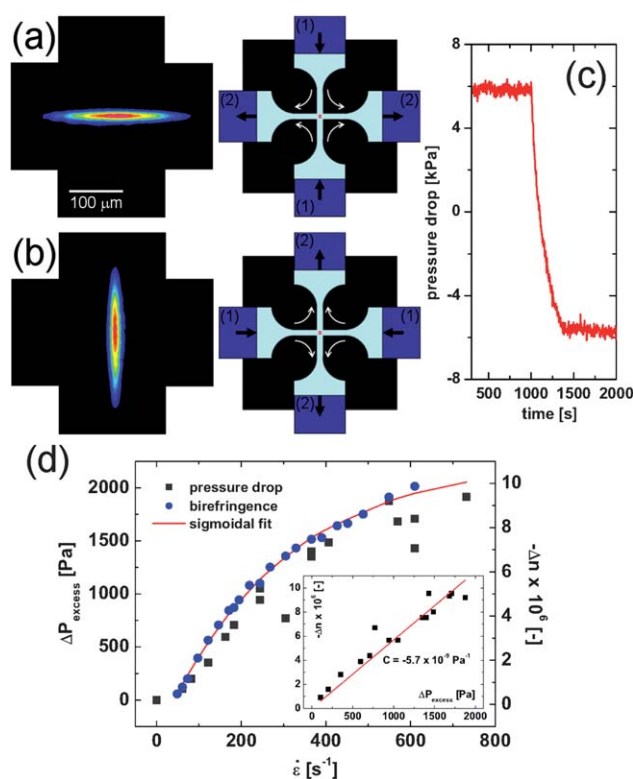**Fig. 3** False colour images of birefringence observed in the cross-slots with a dilute 0.03 wt.% ($c/c^* \sim 1/6$) solution of a low polydispersity sample of 10.2×10^6 g mol^{-1} a-PS in DOP flowing at a strain rate of $\dot{\varepsilon} = 1025$ s^{-1}, $De \sim 2.3$ (piezo voltage $V = 50$ V, period $T = 2$ s). Shown alongside (to the right) are schematic representations of the corresponding piezo pump displacements, (1) represents an extending piezo and (2) represents a retracting piezo. The white arrows indicate the flow direction and the red cross denotes the stagnation point. In (a) the flow enters through the top and bottom channels and exits through the left and right channels; and *vice-versa* in (b). (c) Indicates how the pressure drop varies when flow changes direction. For this particular polymer solution, the time required for the pressure to stabilise was ~ 250 ms. (d) Measured birefringence (Δn) and excess pressure drop ($\Delta P_{excess} = \Delta P_{total} - \Delta P_{shear}$) as a function of strain rate, with (inset) birefringence as a function of excess pressure drop, where the gradient of the straight-line fit gives the stress-optic coefficient, C. Experiment conducted at 22 °C.

Pa^{-1}.[77–80] It is surprising that the SOR appears to hold under conditions of strong stagnation point flow, where the birefringence is close to saturation and we may expect that polymer chains are approaching their limit of extension.[81] In fact such surprising robustness of the SOR for dilute a-PS/DOP solutions undergoing strong extensional flows has been reported before,[80] and shown to remain valid long after finite extensibility models predict its failure.

Fig. 3d lends support to the use of eqn (6) to determine the extensional viscosity, since it indicates that ΔP_{excess} is indeed proportional, and probably equal, to the extensional stress in the birefringent strand. Conversely, the linear relationship between Δn and ΔP_{excess} allows for simple conversion between the two, so that η_E may be computed equally well using either measure.

The effect of progressively lower polymer concentrations on the measured birefringence within the cross-slot is illustrated by

Fig. 4, which shows birefringent strands observed in the ultra-dilute a-PS/DOP solutions. In dilute solutions of non-interacting chains, the apparent extensional viscosity and stress contribution from chain deformation should be proportional to concentration. In these ultra-dilute solutions, even though birefringence is measured, the pressure sensors do not register any measurable excess pressure. It must be noted in Fig. 4 that the strands of stretched polymer molecules are highly localised along the horizontal outflow axis of the cross-slot, since streamlines along this axis must pass close to the stagnation point where both the strain rate and the residence time are at a maximum. The birefringence disappears near to the channel entrances since this marks the edge of the area illuminated by the circular laser beam. Other experiments have shown that in fact the birefringence persists along the length of the outlet channel.[15] The dark, approximately circular regions, on the images correspond to the position of the laser beam, and are caused by stress birefringence in the glass windows of the flow cell. Also, we note that there are some interference fringes on the images. However, we point out that the magnitude of the retardation being detected in the polymer solutions is as low as ~ 0.05 nm in Fig. 4d, so it could be considered remarkable that this is visible above the background noise at all. To the best of our knowledge this is the lowest concentration solution of polymer in which flow induced birefringence has been reported to date. The previous lowest concentration reported that we are aware of was 10 ppm or 0.001 wt.%, which was achieved in an earlier version of the EFOR apparatus.[14]

Values of the birefringence (Δn, measured at the stagnation point) for the ultra-dilute a-PS solutions are presented as a function of the strain rate in Fig. 5a. The birefringence increases rapidly from 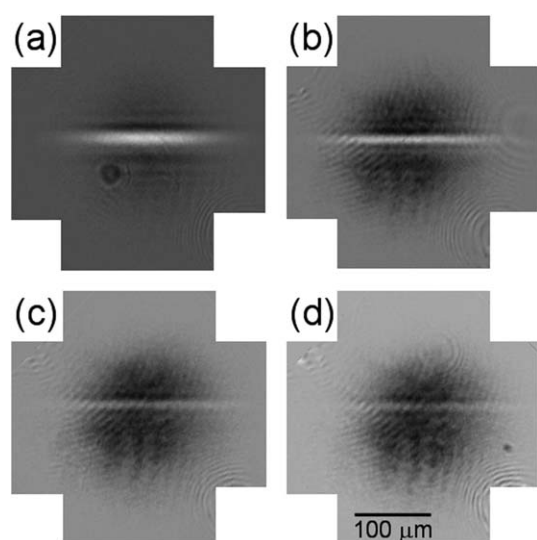zero at low strain rate toward plateau values, which scale well with concentration, as expected for dilute solutions. This is confirmed by the inset in Fig. 5a showing the extension ratio *versus* strain rate, determined using the model derived by Treloar, based on an approximation to the inverse Langevin function and the optical properties of strained networks.[46,82] At the plateau the extension ratio, $\beta = r/L$ (where r = end-to-end separation and L = contour length) is $\beta \sim 0.6$, indicating that the ensemble average end-to-end separation for molecules along the optical path is 0.6 times the contour length.

It should be noted that while previous authors have reported essentially complete chain stretching of macromolecules (*i.e.* fluorescently labelled DNA) in cross-slot flows,[43,44] this applies to individual molecules only. Many molecules that pass through the stagnation point become trapped in metastable 'kinked', 'folded' or 'dumbbell' conformations, due to their orientation as they enter the extensional flow field.[44] In fact no two molecules deform in precisely the same manner leading to the concept of 'molecular individualism'.[83] The ensemble average extension from these experiments is thus considerably less than fully extended, reaching ratios of $\beta = r/L \sim 0.7$ at high strain rates. An interesting question to consider in relation to the present birefringence measurement is: how many polymer molecules does the laser light sample on its passage through the cross-slot? An estimate can be made from the number of molecules per unit volume in the solution. The 0.0002 wt.% a-PS solution contains ~ 2 g m^{-3} of polymer, which is equivalent $\sim 2 \times 10^{-7}$ moles or $\sim 1.2 \times 10^{17}$ polymer molecules per cubic meter. The spatial resolution of the images in Fig. 4 is ~ 1.3 μm/pixel, so each pixel represents a surface area of $\sim 1.7 \times 10^{-12}$ m^2 and a volume of $\sim 1.7 \times 10^{-15}$ m^3. Such a volume should contain ~ 200 polymer molecules. The value of $\beta \sim 0.6$ is in reasonable agreement with the ensemble average extension ratio reported for fluorescently labelled DNA.[43,44]

Further information can be extracted from birefringence measurements such as those in Fig. 5a. As the strain rate is increased so progressively shorter molecules in the (narrow, but finite) molecular weight distribution become stretched, in accordance with the Zimm model for flexible chains in a theta solvent for which the stretching characteristic time $\tau_Z \propto M^{3/2}$.[31] Differentiating Δn with respect to $\dot{\varepsilon}$ and plotting the result against $\tau_{c-s} = 1/\dot{\varepsilon}$, gives a curve of the form shown in Fig. 5b, for the 0.001% a-PS solution. This provides a spectrum of characteristic relaxation times corresponding to the spread of molecular weights present in the distribution. The point of inflection in the Δn *versus* $\dot{\varepsilon}$ curve occurs at the strain rate at which the peak of the molecular weight distribution, $M_p = 10.2 \times 10^6$ g mol^{-1}, stretches. This occurs at a reciprocal strain rate of $\tau_{c-s} \sim 6$ ms. In fact, accounting for shear contributions to the planar extensional flow, Larson and Magda have shown that stretching should occur for $\dot{\varepsilon} > 0.5/\tau_Z$.[84] If we use this scaling we obtain an experimental relaxation time $\tau_{c-s} \sim 3$ ms, in close agreement with the calculated Zimm time $\tau_Z = 2.24$ ms.

The inset of Fig. 5b shows the extension ratio measured as a function of time from birefringence measurements made following the cessation of flow for a slightly more concentrated (0.005 wt.%) solution of a-PS in DOP. The curve has been fitted with a single exponential decay with a time constant equal to the relaxation time from the stretched to the coiled state, $\tau_{s-c} \sim 250$ ms. This is longer than τ_Z by a factor > 100 and is direct

Fig. 4 Birefringence strands observed in the cross-slots for ultra-dilute solutions of $M_p = 10.2 \times 10^6$ gmol^{-1} atactic polystyrene in dioctyl phthalate (a-PS in DOP) at a strain rate of $\dot{\varepsilon} = 400$ s^{-1}, $De = 0.9$. (a) $c = 0.002$ wt.% ($c/c^* \sim 1/100$), (b) $c = 0.001$ wt.% ($c/c^* \sim 1/200$), (c) $c = 0.0005$ wt.% ($c/c^* \sim 1/400$), (d) $c = 0.0002$ wt.% ($c/c^* \sim 1/1000$). Flow enters through the top and bottom channels and exits through the left and right channels. Experiment conducted at 22 °C.
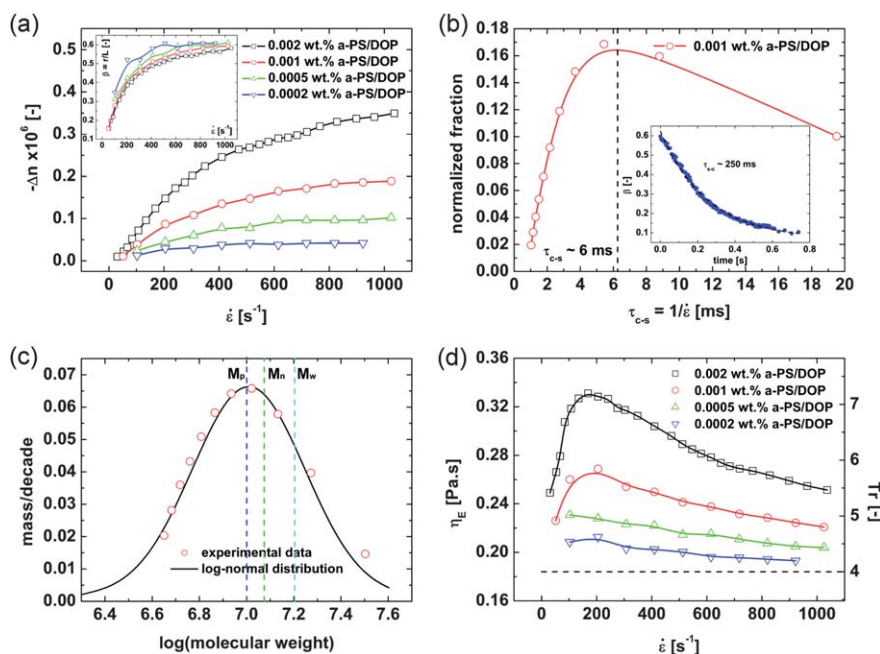
Fig. 5 (a) Birefringence measurements made as a function of strain rate in the cross-slots for ultra-dilute solutions of $M_p = 10.2 \times 10^6$ g mol^{-1} a-PS in DOP. Inset shows the fractional molecular extension derived from birefringence measurements using the Treloar model. (b) Normalized derivative of birefringence plotted against $\tau_{c-s} = 1/\dot{\varepsilon}$, indicating a stretching characteristic time of $\tau_{c-s} \sim 6$ ms for the peak of the molecular weight distribution. Inset shows the decay of fractional molecular extension with time for a 0.05 wt.% solution of $M_p = 10.2 \times 10^6$ g mol^{-1} a-PS in DOP following cessation of flow, fitted with a single exponential decay with a relaxation time of ~ 250 ms. (c) Molecular weight distribution determined from (c), compared with a log-normal distribution with $M_w/M_n = 1.35$. (d) Apparent extensional viscosity and Trouton ratio for ultra-dilute a-PS/DOP solutions derived from (a) using the stress-optical rule with coefficient $C = -5 \times 10^{-9}$ Pa^{-1}, the dashed line indicates $Tr = 4$, which is expected for Newtonian fluids in planar extensional flow. Experiments conducted at 22 °C.

evidence of the coil–stretch hysteresis predicted in 1974 by de Gennes[29] and Hinch.[30] Coil–stretch conformational hysteresis was also reported by Schroeder *et al.* with fluorescently labelled DNA in a cross-slot.[45,85] However, the increase in relaxation time between coiled and stretched states was very small (a factor of only 2×). The reason for this difference is readily explained by DNA in water being a much more expanded coil than a-PS in DOP, due to its high persistence length (~ 50 nm[86]). Thus the change in hydrodynamic interactions between chain segments as DNA stretches is relatively small. This is shown by the requirement of very long DNA molecules (1.3 mm, with $\sim 20,000$ persistence lengths) for hysteresis to be observed. Recently, Larson has discussed the difficulty of quantifying coil-stretch relaxation time hysteresis in dilute solutions of flexible polymer solutions using filament stretching type rheometers.[87] In contrast, we find that in the EFOR such a measurement can be obtained with relative ease.

Previous experiments with a-PS samples of various molecular weight have confirmed the Zimm model to hold for a-PS in theta solvents such as DOP.[15,88,89] Hence, by taking the *x*-axis of Fig. 5b to the power 2/3, it is possible to obtain the molecular weight distribution of the polymer sample, as shown in Fig. 5c.[14,90] Arbitrarily setting $M_p = 10.2 \times 10^6$ g mol^{-1} and fitting a log-normal function to the experimental data, M_w and M_n can be extracted. The experimentally determined values give $M_w/M_n \sim 1.35$, slightly higher than the value of 1.17 quoted by the polymer supplier. This is likely due to the high sensitivity of the technique to the high molecular weight tail of the molecular

weight distribution, where Δn increases rapidly with $\dot{\varepsilon}$. Such high molecular weight tails can significantly affect rheological properties of fluids, especially in extension, but are difficult to detect by GPC. We must also emphasize that the volume of sample required for carrying out this estimate of molecular weight distribution is quite small, and indeed, a single experiment in EFOR provides both the static (size polydispersity) and dynamic (extensional viscosity and relaxation time) measurements.

As mentioned earlier, due to the extremely high dilution of the solutions the pressure drop obtained in extensional flow was not measurably different from the pressure drop measured in shear. However, we can obtain an estimate of the apparent extensional viscosity of the solutions using the stress-optical rule (SOR), $\sigma_{ext} = \Delta n/C$, where σ_{ext} is the stress and C is the stress optical coefficient (we use $C = -5 \times 10^{-9}$ Pa^{-1} for a-PS in DOP[79,91]). Dividing the extensional stress by the extensional strain rate ($\dot{\varepsilon}$) gives the extensional viscosity (η_E) shown in Fig. 5d. The Trouton ratio (Tr) shown on the right hand axis is defined as the ratio of extensional to shear viscosity ($Tr = \eta_E/\eta_{shear}$). $Tr = 4$ for Newtonian fluid in planar extensional flow, marked by the dashed grey line in Fig. 5d. The extensional viscosity and Tr for the two more concentrated polymer solutions increases at low strain rates up to a peak value at $\dot{\varepsilon} \sim 200$ s^{-1}, before showing an apparent reduction. The Deborah number at the peak of η_E is $De = \dot{\varepsilon}\tau_Z \sim 0.5$. The most dilute solutions simply show a slowly decaying extensional viscosity with strain rate. In fact at 0.0002 wt.% the fluid appears essentially Newtonian, which is not surprising. 0.0002 wt.% is below the critical minimum concentration derived by Clasen

et al.[52] ($c_{min} = M_w\eta_S C_\infty/2RT\tau_Z n$, where R is the ideal gas constant), below which the polymer is expected to carry less stress than the solvent even when molecules are fully extended. For our fluid $c_{min} \sim 0.0004$ wt.%. We do not believe the reduction in apparent extensional viscosity beyond $\dot{\varepsilon} \sim 200\,s^{-1}$ can be explained by inertial effects or by flow-induced scission of polymer chains. Here inertial effects are small since the Reynolds number is $Re \sim 0.1$ at the strain rate where the reduction in extensional viscosity begins. Flow induced chain scission is discounted since fresh fluid was loaded into the flow cell following the collection of each individual data point, and no reduction in the birefringence was noticed between pump cycles. In addition the measured birefringence itself (Fig. 5a) continues to increase smoothly to strain rates significantly beyond $\dot{\varepsilon} \sim 200\,s^{-1}$ and we do not obtain a bimodal molecular weight distribution, which is a signature of polymer degradation.[92] Flow perturbation[16] and transient entanglement arguments[93] can not be made due to the ultra-dilute nature of the polymer solutions. Additionally, we cannot invoke failure of the stress-optical rule, as we can see from Fig. 3d that the SOR holds up to strain rates of at least $\dot{\varepsilon} \sim 600\,s^{-1}$.

In fact, extensional thinning has been observed in many experiments with dilute and concentrated polymer solutions,[15,16,94–97] as well as in simulations.[87,97,98] However, Brownian dynamics simulations for dilute solutions using bead-spring or bead-rod models in a continuum solvent (see discussion by Larson[87]) as well as most multimode, differential constitutive models[99] show that extensional viscosity increases with extension rate, and then saturates to a steady state value as macromolecules achieve full extension. In fact the constitutive models – Bird-DeAguir, Giesekus and Acierno, Lamantia, Marrucci and Titomanlio (ALMT) – all give a constant steady state value for extensional viscosity, while the Upper Convected Maxwell (UCM) and White-Metzner (WM) models predict an extensional viscosity that grows without bound, as summarized by Quizani *et al.*[97] and Bird *et al.*[99] Experiments on melts and concentrated solutions also show extensional thinning beyond a critical strain or strain rate and constitutive models like the Wiest model[100] that incorporates finite extensibility along with anisotropic hydrodynamic drag can capture extensional thinning.[100–102] Additional effects like chain entanglements affect the response to elongational flow in melts or concentrated solutions, and we will limit this discussion to dilute solutions only. For dilute solutions, Gupta, Nguyen and Sridhar[95] experimentally measured extension thinning at $De_{GNS} > 10$ (using a relaxation time measured in shear experiments, which is therefore close to the Zimm time). Gupta *et al.* used the Wiest model to capture the extensional thinning behaviour and found that the limiting extensional viscosity scaled as $\eta_E \propto De_{GNS}^{-\alpha}$, where $\alpha = 0.5$. Interestingly, in non-equilibrium Monte Carlo simulations using a Bond Fluctuation model, Li and Denn[98] showed that both the coil-stretch transition and extensional thinning are manifested beyond $De_{LD} > 0.5$ (based on a time scale needed for relaxation from a fully extended chain, which is closer to a Rouse relaxation time). In these simulations, the extensional stress saturates at high rates, as the possible microstates for a fully extended chain in lattice are limited, implying that the entropic stress is bounded, and therefore extensional thinning is caused by finite extensibility of the chain. While Li and Denn define the critical extension rate using a relaxation time where hydrodynamic interactions (HI's)

are ignored, Gupta *et al.* suggest that the role of HI's becomes less prominent for high extension rate flows of dilute polymer solutions. The Wiest model invokes anisotropic drag in addition to finite extensibility, which at the molecular level can arise due to deformation-dependent drag, as the value of pre-averaged HI's invoked by Zimm's model is applicable only for coils. The dependence of HI's on polymer deformation or relative configuration of polymer segments was predicted by de Gennes in 1974[29,87] and also leads to the criticality of the coil-stretch transition. The underlying physics that drives the extensional thinning at high rates $De_{GNS} > 10$ or $De_{LD} > 0.5$ (irrespective of the constitutive model used for analysis or simulation) and initial rise in extensional viscosity with extension rate is due to coupling of elastic (bounded by finite extensibility) and viscous effects, (the overall drag depends on the instantaneous configuration and HI's in the coils under consideration). The critical extension rate at which the coil-stretch transition occurs thus depends upon relaxation time (and hence the molecular weight for the chain), and in any experiment chains of different length undergo coil-stretch transitions at different rates dictated by individual relaxation times. The cumulative effect of coil–stretch transitions of chains in a polydisperse sample is observed in the experiments described here, whereby the rate-dependence of extensional viscosity in the extension thinning regime shows a power law dependence (or $\eta_E \propto \dot{\varepsilon}^{-\alpha}$ where $\alpha < 0.5$) and is seen to be a function of concentration.

Aqueous bio-polymer solutions

Hyaluronic acid. Aqueous biopolymer solutions are primary ingredients in a wide variety of applications including foods, eye drops, consumer care products and prosthetic fluids.[103] The effectiveness of such fluids in *e.g.* mimicking real physiological fluids could be improved greatly if their extensional properties as well as shear rheological properties could be matched.[21] To demonstrate the application of the EFOR to measuring the properties of biological fluids, Fig. 6 shows the optical response of a 0.1 wt.% solution of a high molecular weight hyaluronic acid (HA) in a physiological PBS buffer. While not as sharply defined as the birefringent strands observed in a-PS/DOP solutions, the birefringence in Fig. 6 is quite localized along the stagnation point streamline, where fluid strains are highest, consistent with the expected flexible to semi-flexible conformation of HA in PBS.[61,63]

The birefringence (Δn) and excess pressure drop (ΔP_{excess}) measured in the HA solution as a function of the nominal strain rate, $\dot{\varepsilon}$ are shown in Fig. 7a. Both increase approximately linearly with $\dot{\varepsilon}$. This linear increase is indicative of either a very broad molecular weight distribution, and/or non-critical stretching of the HA. The corresponding stress-optical diagram for HA solutions is shown in the inset of Fig. 7a; the stress-optical coefficient can be read off from the slope giving $C = 5.9 \times 10^{-8}$ Pa^{-1}. The stress optical coefficient for HA in PBS solutions was reported only recently by Kulicke and coworkers[104] in steady shear and our value is indeed comparable to their value of $C = 1.82 \times 10^{-8}$ Pa^{-1}. Also shown on Fig. 7b are the shear and extensional viscosities determined from the measured pressure drop using eqn (5) and (6), respectively. The shear viscosity is only slightly higher than water at ~ 2 mPa s, however the
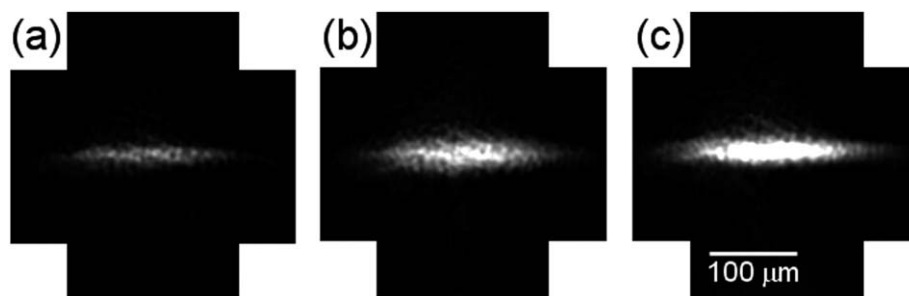
Fig. 6 Birefringence observed in the cross-slots for a 0.1 wt.% solution of hyaluronic acid dissolved in a phosphate buffered saline (PBS) (a) $\dot\varepsilon = 1230\ s^{-1}$, (b) $\dot\varepsilon = 2050\ s^{-1}$, (c) $\dot\varepsilon = 3280\ s^{-1}$. Flow enters through the top and bottom channels and exits through the left and right channels. Experiment conducted at 22 °C.

extensional viscosity is significantly higher than that, increasing rapidly from a very low strain rate up to a plateau value of ∼ 20 mPa s, giving a Trouton ratio of ∼10. This Trouton ratio is similar to values reported previously using an opposed-jet rheometer,[58] however it is lower by a factor of ∼10 than recently reported values for similar fluids tested in a capillary break-up extensional rheometer.[105] This discrepancy may be at least partially accounted for by flow modification around the stagnation point of the cross-slot. If the strain rate drops below the nominal value, this leads to an error in eqn (6) and an underestimate of η_E.[15,16] Although a Trouton ratio of 10 is fairly modest, in synovial fluid the concentration of HA is thought to be about 3× higher than in the solution tested here[106] and the molecular weight is also higher.[107]

As for the model a-PS/DOP solution, we can smooth and differentiate the birefringence vs. strain rate curve for HA to

obtain a spectrum of characteristic relaxation times for the sample. This is shown in Fig. 7c, which gives a peak at $\tau_{c-s} \sim 1.3$ ms.

Also, bearing in mind that the solvent quality of PBS for HA is not clear, and the HA macromolecules may not obey perfect Zimm-like behaviour in solution (i.e. that $\tau_{c-s} \propto M^{1.5}$), we proceed, as for the model a-PS sample to rescale the data of Fig. 7c to obtain the molecular weight distribution of the HA sample (Fig. 7d). Indeed, Odell and Keller [90] have argued that although the absolute value of τ_{c-s} depends on solvent quality, in extensional flows its functional dependence on M always obeys Zimm-like behaviour. This seems to be corroborated by extensional flow experiments with well-defined polymer samples in solvents of various quality.[90,108,109] A theoretical basis for the understanding of the apparent universality of Zimm dynamics in extensional flows was forwarded by Rabin,[110] who argues that extensional flow experiments probe the dynamics of the partially
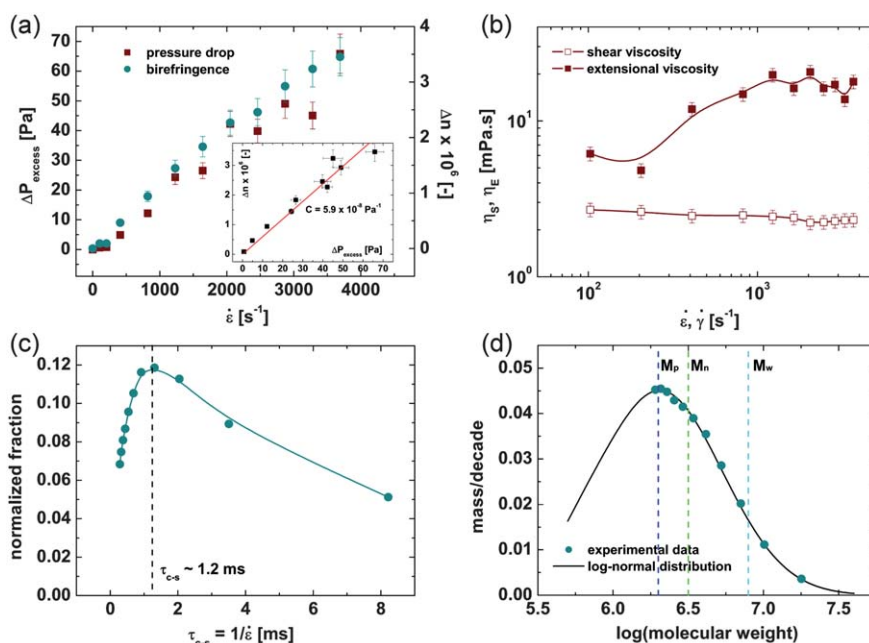

Fig. 7 (a) Excess pressure drop and birefringence (measured at the stagnation point) as a function of strain rate for 0.1 wt.% hyaluronic acid in PBS. Inset: Birefringence as a function of excess pressure, showing an estimate of the stress-optical coefficient, C. (b) Apparent shear and extensional viscosities for 0.1 wt.% hyaluronic acid in PBS, determined from pressure drop measurements in the cross-slots. (c) Relaxation time spectrum for the HA sample, determined from birefringence measurements, showing the relaxation time of the peak of 1.2 ms. (d) Molecular weight distribution of the HA sample determined from birefringence measurements fitted with a log-normal distribution. Experiment conducted at 22 °C.

stretched coil. In Fig. 3d, the same scaling factor has been used as for the 10.2×10^6 g mol^{-1} a-PS GPC calibration standard. The resulting log-normal distribution has a peak at $M_p \sim 2 \times 10^6$ g mol^{-1}, close to the nominal value of $3–4 \times 10^6$ g mol^{-1} specified by the supplier. Again the discrepancy may be accounted for by flow modification; if the strain rate were lower than expected this would give a higher molecular weight. The log-normal fit to the HA data gives a value of $M_w/M_n \sim 2.5$.

Saliva. Next we tested saliva samples in the EFOR. Saliva not only has highly interesting and poorly understood rheological properties, worthy of investigation in their own right, but also serves as a prototypical example of a mucosal fluid[111] and allows us to demonstrate the use of the EFOR technique with a genuine physiological fluid. The optical response of a typical sample of healthy human saliva is shown in Fig. 8. At low strain rates (e.g. $\dot{\varepsilon} \sim 400$ s^{-1}, Fig. 8a) the birefringence is fairly localized along the stagnation point streamline, however with increasing strain rate the birefringent region broadens significantly (Fig. 8b) until it occupies a significant proportion of the channel width (e.g. $\dot{\varepsilon} \sim 3300$ s^{-1}, Fig. 8c). The degree of localization of birefringence around the stagnation point depends strongly on the macromolecular flexibility. Flexible polymers such as a-PS, require high strains to stretch and the birefringence is localised along streamlines close to the stagnation point where the fluid strain is highest. Stiffer molecules require less strain to achieve a high stretching, and hence can give a birefringent response along streamlines that pass far from the stagnation point.[112] The high molecular weight mucins in saliva, which are the molecules most likely to be stretching in the flow, are stiffened by densely packed oligosaccharide side-groups linked to the main protein backbone and by repulsive negative backbone charges.[56,67]

The birefringence measured at the stagnation point is plotted as a function of the strain rate in Fig. 9a. The data is averaged over four individual saliva samples and the error bars represent the standard deviation. The birefringence was measurable down to a strain rate of ~ 50 s^{-1}, indicating a relaxation time for the longest mucin molecules of at least ~ 20 ms. Initially the birefringence increases rapidly with strain rate, however the increase becomes more gradual after $\dot{\varepsilon} \sim 100$ s^{-1} and plateaus at a value of $\Delta n \approx 8 \times 10^{-7}$ after $\dot{\varepsilon} \sim 1000$ s^{-1}. Fig. 9a also shows the measured excess pressure drop for the saliva, which in this case clearly does not scale linearly with the birefringence. This behaviour indicates that the mucin molecules readily orient in the flow field for little applied stress, resulting in a high birefringence. However, once

aligned in the flow direction, a high stress is required to cause further stretching and orientation. The result is a stress-optical coefficient that decreases with strain rate. This behaviour is again characteristic of fairly rigid or wormlike molecules,[113] consistent with the observations of broadening of the birefringent band. The inset in Fig. 9a shows the stress-optical curve determined for saliva, and the nonlinearity in the extensional response is clearly apparent here. Using the initial slope of the stress-optical curve, we estimate the stress optical coefficient of saliva, at low stress and low strain rate, to be $C = 1.1 \times 10^{-7}$ Pa^{-1}, which we believe is the first such measurement. Such data could be useful for the rapid quantitative characterization of the elastic properties of saliva samples based solely on their optical properties at low deformation rates.

The apparent extensional viscosity of saliva is computed using the measured excess pressure drop as a function of extension rate, and the Trouton ratio, $Tr = \eta_E/\eta_{shear}$, of the saliva sample is shown in Fig. 9b. Tr reaches a peak value of ~ 25 at $\dot{\varepsilon} \sim 400$ s^{-1} before showing a progressive reduction. The peak Trouton ratio shows that saliva has very significant extensional properties. It should be recalled that the saliva samples were centrifuged prior to testing, which is likely to have caused the loss of some mucin. Consequently whole raw saliva would likely show a higher Trouton ratio than reported here. The dramatic reduction in Trouton ratio beyond $\dot{\varepsilon} \sim 2000$ s^{-1}, may indicate a number of phenomena. It is likely that the flow is being significantly perturbed by the broadening of the elastic strand; if the actual strain rate at the stagnation point drops below the nominal value, $\dot{\varepsilon}$, this leads to an error in eqn (6) and an underestimation of η_E. In such cases it is desirable to perform complementary particle image velocimetry in order to directly measure the true strain rate at the stagnation point.[15,16] An alternative explanation is flow-induced scission of the disulphide bonds that link individual mucin molecules, however this is thought to be unlikely since fresh saliva was injected into the cross-slot after collection of each data point. We can speculate on the reasons for the high elasticity of saliva. The elastic property is likely to be of great importance to the functionality of saliva in terms of lubrication and surface adhesion within the oral cavity and in binding of the bolus when masticating. It is also likely to have a significant impact on texture perception in the mouth during processing and consumption of food and drinks.[114–116] This should be taken into account in the formulation of artificial salivas for the treatment of dry mouth conditions.
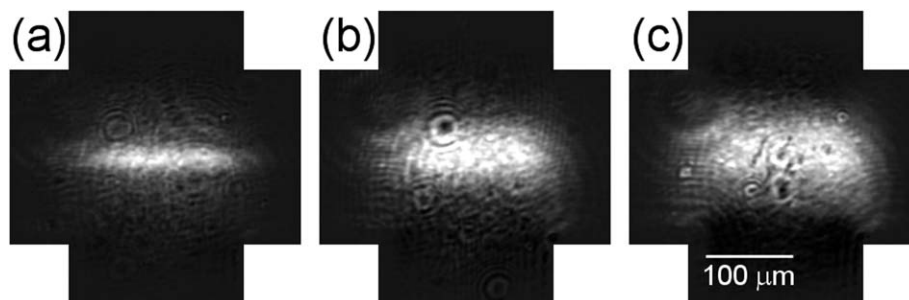

Fig. 8 Birefringence observed in the cross-slots for a centrifuged sample of fresh human saliva (a) $\dot{\varepsilon} = 410$ s^{-1}, (b) $\dot{\varepsilon} = 1640$ s^{-1}, (c) $\dot{\varepsilon} = 3280$ s^{-1}. Flow enters through the top and bottom channels and exits through the left and right channels. Experiment conducted at 22 °C.
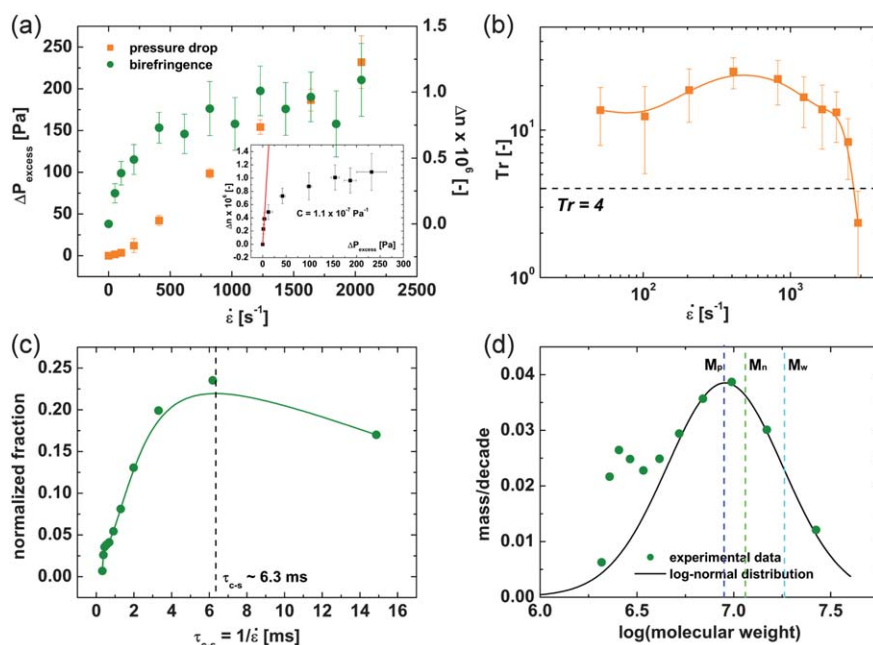
Fig. 9 (a) Excess pressure drop and birefringence (measured at the stagnation point) as a function of strain rate for saliva. Inset: Birefringence as a function of excess pressure, showing an estimate of the stress-optical coefficient, C. (b) Trouton ratio for saliva, determined from pressure drop measurements in the cross-slots. The dashed line represents the Trouton ratio expected for a Newtonian fluid in planar extensional flow. (c) Relaxation time spectrum for the saliva sample, determined from birefringence measurements, showing the relaxation time of the peak of ~6 ms. (d) Molecular weight distribution of the saliva sample determined from birefringence measurements and fitted with a log-normal distribution. Experiment conducted at 22 °C.

Smoothing the birefringence *vs.* strain rate data, differentiating and plotting against $1/\dot{\varepsilon}$, gives the spectrum of relaxation times for saliva shown in Fig. 9c. Here we find a peak at $\tau_{c\text{-}s} \sim 6.3$ ms. Scaling the axes to give a molecular weight distribution we obtain Fig. 9d, again we have used the same scaling factor as for the a-PS and HA samples. Here a log-normal distribution can again be fitted, giving a value of $M_p \sim 9 \times 10^6$ g mol^{-1} and $M_w/M_n \sim 1.6$. Satisfyingly, the spread of the log-normal distribution spans the molecular weight range expected for salivary mucins.[64] Intriguingly, there is a low molecular weight shoulder on the experimental data. Although the raw birefringence data is noisy in this region (high $\dot{\varepsilon}$ part) it is tempting to explain this apparent bimodal distribution as the stretching of two different mucin species within the saliva. The main peak at 9×10^6 g mol^{-1} is almost certainly due to the stretching of MUC5B mucins, which are by far the highest molecular weight molecules in saliva.[64] A possible candidate for the second, low molecular weight peak, which occurs at around 2.5×10^6 g mol^{-1} is MUC16, which has been reported to have approximately this molecular weight.[117]

We end this section by mentioning that apart from stagnation point flows, a number of methods have been devised for the study of fluids under extensional flows. The capillary break-up (CaBER) and filament stretching (FiSER) extensional rheometers are excellent techniques when applied to high viscosity or highly elastic fluids which can support a thread and minimise gravitational sagging.[118,119] Progress is also being made towards the application of CaBER to lower viscosity fluids[120,121] and lower polymer concentrations.[52,121] However, free-surface phenomena such as 'beads-on-a-string' formation,[122] and 'necking' (*i.e.* capillary)[123] or end-plate[124] instabilities, that lead to break-up of the filament, limit the range of applicable fluids.

Also, the scale of the FiSER apparatus is such that both solvent volatility and temperature control become important and non-trivial issues. In addition many biological fluids contain surface active molecules that can adsorb to the air–liquid interface in such devices, which could lead to anomalous results.[114,125,126] The recent development of the microfluidic extensional rheometer based on flow through a hyperbolic contraction holds some promise for the study of suitable fluids,[24] however such devices suffer from only providing a limited Hencky strain to the fluid (due to the transience of the flow and the fixed contraction ratio) and also the tendency of the flow to become asymmetric or develop vortices at rather low volumetric flow rates and hence strain rates. Additionally, the separation of shear and extensional contributions to the measured quantities (*i.e.* the pressure drop) is highly complex, which restricts the instrument to the category of an 'indexer' as opposed to a true extensional rheometer. The EFOR, while also having its own limits, provides an extensional rheometry technique that can bridge some of the gaps left by these other devices, having particular applications to the rheology of dilute solutions and biofluids.

4. Conclusions

The use of the optomicrofluidic technique of cross-slot extensional flow oscillatory rheometry (EFOR) provides the simultaneous measurement of excess pressure drop and birefringence resulting from macromolecular deformation in an extension flow field. By confining a few microlitres of fluid about a stagnation point within a cross-slot geometry, the stress optical diagram for model polystyrene solutions was constructed and the stress optical coefficient was computed. For the ultra-dilute solutions

the excess pressure drop is miniscule, and not detected by the pressure sensors, though the effect of added polymer is visible in the presence of a birefringence signal. We use the stress optical coefficient to quantify the apparent extensional stress and compute the apparent extensional viscosity of ultra-dilute solutions. It must be noted here that the concentrations used in this study are lower than accessed by most conventional techniques and we present birefringence signal and extensional response from unprecedentedly low polymer concentrations. The visualization and measurement of birefringence of a polymer solution around stagnation point provides a ready tool to corroborate molecular theories of polymer dynamics. In the present study, we are able to distinguish a coil-stretch transition and coil-stretch hysteresis in polystyrene solutions. Though the maximum elongation observed is only up to 60% of the contour length, unlike single molecule experiments on DNA, the birefringence measured from a-PS/DOP solutions averages over an ensemble of molecules and hence on average full extension is not realized.

We extract the extensional response and stress optical coefficient of hyaluronic acid and saliva, reporting probably the first value of SOC for saliva. Both HA and saliva are commonly found body fluids that are often replaced by synthetic analogues, where the standard industry practice is to match the shear rheology only. We anticipate that the design of functional synthetic analogues of body fluids will require the same exquisite control of extensional viscosity that is currently incorporated in case of shear viscosity, hydrophilicity, etc. The possibility of using a few microlitres of sample for quantitative assessment of body fluids is encouraging for diagnostic applications where the amount of sample volume is severely restricted.

Acknowledgements

References

1 F. T. Trouton, *Proc. R. Soc. London, Ser. A*, 1906, **77**, 426–440.
2 C. J. S. Petrie, *Elongational Flows*, Pitman Publishing Ltd, London, 1979.
3 C. J. S. Petrie, *J. Non-Newtonian Fluid Mech.*, 2006, **137**, 1–14.
4 V. Tirtaatmadja and T. Sridhar, *J. Rheol.*, 1993, **37**, 1081–1102.
5 D. F. James and T. Sridhar, *J. Rheol.*, 1995, **39**, 713–724.
6 A. G. Fabula, J. W. Hoyt and H. R. Crawford, *Bulletin, American Physical Society*, 1963, 8.
7 P. S. Virk and H. Baher, *Chem. Eng. Sci.*, 1970, **25**, 1183–1189.
8 D. L. Dauben and D. E. Menzie, *JPT, J. Pet. Technol.*, 1967, **19**, 1065–1073.
9 R. J. Marshall and A. B. Metzner, *Ind. Eng. Chem. Fundam.*, 1967, **6**, 393–400.
10 P. P. Bhat, S. Appathurai, M. T. Harris, M. Pasquali, G. H. McKinley and O. A. Basaran, *Nat. Phys.*, 2010, **6**, 625–631.
11 L. Gaume and Y. Forterre, *PLoS One*, 2007, **2**, 1–7.
12 V. Sahni, T. A. Blackledge and A. Dhinojwala, *Nat. Commun.*, 2010, **1**, 1–4.
13 N. Kojic, J. Bico, C. Clasen and G. H. McKinley, *J. Exp. Biol.*, 2006, **209**, 4355–4362.
14 J. A. Odell and S. P. Carrington, *J. Non-Newtonian Fluid Mech.*, 2006, **137**, 110–120.
15 S. J. Haward, J. A. Odell, Z. Li and X.-F. Yuan, *Rheol. Acta*, 2010, **49**, 633–645.
16 S. J. Haward, J. A. Odell, Z. Li and X.-F. Yuan, *Rheol. Acta*, 2010, **49**, 781–788.
17 S. J. Haward, *Rheol. Acta*, 2010, **49**, 1219–1225.
18 S. J. Haward, J. A. Odell, M. Berry and T. Hall, *Rheol. Acta*, 2011, DOI: 10.1007/s00397-010-0494-1.
19 M. Mackley, *Rheol. Acta*, 2010, **49**, 443–458.
20 L. E. Rodd, T. P. Scott, D. V. Boger, J. J. Cooper-White and G. H. McKinley, *J. Non-Newtonian Fluid Mech.*, 2005, **129**, 1–22.
21 P. C. Sousa, F. T. Pinho, M. S. N. Oliveira and M. A. Alves, *Biomicrofluidics*, 2011, **5**, 014108.
22 J. Soulages, M. S. N. Oliveira, P. C. Sousa, M. A. Alves and G. H. McKinley, *J. Non-Newtonian Fluid Mech.*, 2009, **163**, 9–24.
23 S. J. Haward and J. A. Odell, *Rheol. Acta*, 2004, **43**, 350–363.
24 C. J. Pipe and G. H. McKinley, *Mech. Res. Commun.*, 2009, **36**, 110–120.
25 V. Tirtaatmadja, G. H. McKinley and J. J. Cooper-White, *Phys. Fluids*, 2006, **18**, 043101.
26 A. Ardekani, V. Sharma and G. H. McKinley, *J. Fluid Mech.*, 2010, **665**, 46–56.
27 T. J. Sridhar, *J. Non-Newtonian Fluid Mech.*, 1990, **35**, 85–92.
28 D. F. James and K. Walters, in *Techniques of Rheological Measurement*, ed. A. A. Collyer, Elsevier, New York, 1994, vol. 33.
29 P. G. De Gennes, *J. Chem. Phys.*, 1974, **60**, 5030–5042.
30 E. J. Hinch, Polymeres et Lubrification, *Colloques Internationaux du CNRS*, 1974, **233**, 241–247.
31 B. H. Zimm, *J. Chem. Phys.*, 1956, **24**, 269–278.
32 P. E. Rouse, *J. Chem. Phys.*, 1953, **21**, 1272–1280.
33 G. K. Batchelor, *J. Fluid Mech.*, 1970, **44**, 419–440.
34 D. R. Link, S. L. Anna, D. A. Weitz and H. A. Stone, *Phys. Rev. Lett.*, 2004, **92**, 054503.
35 S. D. Hudson, F. R. Phelan, M. D. Handler, J. T. Cabral, K. B. Migler and E. J. Amis, *Appl. Phys. Lett.*, 2004, **85**, 335–337.
36 J. S. Lee, E. S. G. Shaqfeh and S. J. Muller, *Physical Review E*, 2007, **75**, 040802.
37 J. S. Lee, R. Dylla-Spears, N. P. Teclemariam and S. J. Muller, *Appl. Phys. Lett.*, 2007, **90**, 074103.
38 J. Deschamps, V. Kantsler, E. Segre and V. Steinberg, *Proc. Natl. Acad. Sci. U. S. A.*, 2009, **106**, 11444–11447.
39 J. A. Pathak and S. D. Hudson, *Macromolecules*, 2006, **39**, 8782–8792.
40 R. Dylla-Spears, J. E. Townsend, L. Jen-Jacobson, L. L. Sohn and S. J. Muller, *Lab Chip*, 2010, **10**, 1543–1549.
41 P. A. Stone, S. D. Hudson, P. Dalhaimer, D. E. Discher, E. J. Amis and K. B. Migler, *Macromolecules*, 2006, **39**, 7144–7148.
42 O. Scrivener, C. Berner, R. Cressely, R. Hocquart, R. Sellin and N. S. Vlachos, *J. Non-Newtonian Fluid Mech.*, 1979, **5**, 475–495.
43 T. T. Perkins, D. E. Smith and S. Chu, *Science*, 1997, **276**, 2016–2021.
44 D. E. Smith and S. Chu, *Science*, 1998, **281**, 1335–1340.
45 C. M. Schroeder, H. P. Babcock, E. S. G. Shaqfeh and S. Chu, *Science*, 2003, **301**, 1515–1519.
46 J. A. Odell, in *Handbook of Experimental Fluid Mechanics*, ed. C. Tropea, Y. L. Yarin and J. F. Foss, Springer-Verlag, Heidelberg, 2007, pp. 724–732.
47 G. C. Berry, *J. Chem. Phys.*, 1967, **46**, 1338–1352.
48 W. W. Graessley, *Polymer*, 1980, **21**, 258–262.
49 J. Brandrup and E. H. Immergut, *Polymer Handbook*, Wiley Interscience, USA, 1989.
50 V. N. Tsvetkov, V. E. Eskin and S. Y. Frenkel, Structure of Macromolecules in Solution, *National Lending Library for Science and Technology*, Boston Spa, 1971.
51 G. Harrison, J. Remmelgas and L. G. Leal, *J. Rheol.*, 1998, **42**, 1039–1058.
52 C. Clasen, J. P. Plog, W.-M. Kulicke, M. Owens, C. Macosko, L. E. Scriven, M. Verani and G. H. McKinley, *J. Rheol.*, 2006, **50**, 849–881.
53 C. Backus, S. P. Carrington, L. R. Fisher, J. A. Odell and D. A. Rodrigues, in *Hyaluronan Volume 1: Chemical, Biochemical and Biological Aspects*, ed. J. F. Kennedy, O. G. Phillips, P. A. Williams and V. C. Hascall, Woodhead Publishing Ltd, Cambridge, 2002, pp. 209–218.
54 C. J. Fuller, personal communication.
55 A. Maleki, A.-L. Kjoniksen and B. Nystrom, *Macromol. Symp.*, 2008, **274**, 131–140.

56 B. Nystrom, A.-L. Kjoniksen, N. Beheshti, A. Maleki, K. Zhu, K. D. Knudsen, R. Pamies, J. G. Hernandez Cifre and J. G. de la Torre, *Adv. Colloid Interface Sci.*, 2010, **158**, 108–118.

57 M. J. Miles, K. Tanaka and A. Keller, *Polymer*, 1983, **24**, 1081–1088.

58 Y. Mo and K. Nishinari, *Biorheology*, 2001, **38**, 379–387.

59 P. Gribbon, B. C. Heng and T. E. Hardingham, *Biophys. J.*, 1999, **77**, 2210–2216.

60 T. C. Laurent and J. Gergely, *The Journal of Biological Chemistry*, 1955, **212**, 325–333.

61 R. Mendichi, L. Soltes and A. G. Schieroni, *Biomacromolecules*, 2003, **4**, 1805–1810.

62 M. Johnson, R. Kamm, G. R. Ethier and T. Pedley, *PhysicoChemical Hydrodynamics*, 1987, **9**, 427–441.

63 W. E. Krause, E. G. Bellomo and R. H. Colby, *Biomacromolecules*, 2001, **2**, 65–69.

64 D. J. Thornton, N. Khan, R. Mehrotra, M. Howard, E. Veerman, N. H. Packer and J. K. Sheehan, *Glycobiology*, 1999, **9**, 293–302.

65 E. J. Helmerhorst and F. G. Oppenheim, *J. Dent. Res.*, 2007, **86**, 680–693.

66 S. A. Rayment, B. Liu, G. D. Offner, F. G. Oppenheim and R. F. Troxler, *J. Dent. Res.*, 2000, **79**, 1765–1772.

67 K. A. Thomsson, A. Prakobphol, H. Leffler, M. S. Reddy, M. J. Levine, S. J. Fisher and G. C. Hansson, *Glycobiology*, 2002, **12**, 1–14.

68 A. N. Round, M. Berry, T. J. McMaster, S. Stoll, D. Gowers, A. P. Corfield and M. J. Miles, *Biophys. J.*, 2002, **83**, 1661–1670.

69 P. J. Flory, *Statistical Mechanics of Chain Molecules*, Interscience, New York, 1969.

70 A. M. Pedersen, A. Bardow, S. Beier Jensen and B. Nauntofte, *Oral Dis.*, 2002, **8**, 117–129.

71 S. Rossi, M. Marciello, M. C. Bonferoni, F. Ferrari, G. Sandri, C. Dacarro, P. Grisoli and C. Caramella, *Eur. J. Pharm. Biopharm.*, 2010, **74**, 248–254.

72 A. L. Innes, S. D. Carrington, D. J. Thornton, S. Kirkham, K. Rousseau, R. H. Dougherty, W. W. Raymond, G. H. Caughey, S. J. Muller and J. V. Fahy, *Am. J. Respir. Crit. Care Med.*, 2009, **180**, 203–210.

73 D. J. Serisier, M. P. Carroll, J. K. Shute and S. A. Young, *Respir. Res.*, 2009, **10**, 63–70.

74 J. M. Dealy, *Rheology Bulletin*, 2010, **79**, 14–18.

75 T. J. Craven, J. M. Rees and W. B. Zimmerman, *Microfluid. Nanofluid.*, 2010, **9**, 559–571.

76 M. Doi and S. F. Edwards, *The Theory of Polymer Dynamics*, Oxford University Press, New York, 1986.

77 P. S. Doyle, E. S. G. Shaqfeh, G. H. McKinley and S. H. Spiegelberg, *J. Non-Newtonian Fluid Mech.*, 1998, **76**, 79–110.

78 H. Janeschitz-Kriegl, *Polymer Melt Rheology and Flow Birefringence*, Springer-Verlag, Berlin, 1983.

79 D. C. Venerus, S. H. Zhu and H.-C. Ottinger, *J. Rheol.*, 1999, **43**, 795–813.

80 J.-M. Li, W. R. Burghardt, B. Yang and B. Khomami, *J. Non-Newtonian Fluid Mech.*, 2000, **91**, 189–220.

81 G. G. Fuller, *Optical Rheometry of Complex Fluids*, Oxford University Press, New York, 1995.

82 L. K. G. Treloar, *The Physics of Rubber Elasticity*, Clarendon Press, Oxford, 1975.

83 P. G. De Gennes, *Science*, 1997, **276**, 1999–2000.

84 R. G. Larson and J. J. Magda, *Macromolecules*, 1989, **22**, 3004–3010.

85 C. M. Schroeder, E. S. G. Shaqfeh and S. Chu, *Macromolecules*, 2004, **37**, 9242–9256.

86 C. Bustamante, J. F. Marko, E. D. Siggia and S. Smith, *Science*, 1994, **256**, 1599–1600.

87 R. G. Larson, *J. Rheol.*, 2005, **49**, 1–70.

88 S. P. Carrington, J. P. Tatham, J. A. Odell and A. E. Saez, *Polymer*, 1997, **38**, 4151–4164.

89 S. P. Carrington, J. P. Tatham, J. A. Odell and A. E. Saez, *Polymer*, 1997, **38**, 4595–4607.

90 J. A. Odell and A. Keller, *Journal of Polymer Science*, 1986, **24**, 1889–1916.

91 J. P. Rothstein and G. H. McKinley, *J. Non-Newtonian Fluid Mech.*, 2002, **108**, 275–290.

92 J. A. Odell, A. Keller and A. J. Muller, *Colloid Polym. Sci.*, 1992, **270**, 307–324.

93 J. A. Odell, A. Keller and A. J. Muller, in *Polymers in aqueous media*, ed. J. E. Glass, American Chemical Society, Washington, 1989, pp. 193–244.

94 C. A. Cathey and G. G. Fuller, *J. Non-Newtonian Fluid Mech.*, 1988, **30**, 303–316.

95 R. K. Gupta, D. A. Nguyen and T. Sridhar, *Phys. Fluids*, 2000, **12**, 1296–1318.

96 D. M. Jones, K. Walters and P. R. Williams, *Rheol. Acta*, 1987, **26**, 20–30.

97 L. M. Quinzani, R. C. Armstrong and R. A. Brown, *J. Rheol.*, 1995, **39**, 1201–1227.

98 X. Li and M. M. Denn, *J. Rheol.*, 2004, **48**, 805–821.

99 R. B. Bird, R. C. Armstrong and O. Hassager, *Dynamics of Polymeric Liquids*, John Wiley and Sons Inc, New York, 1987.

100 J. M. Wiest, *Rheol. Acta*, 1989, **28**, 4–12.

101 V. H. Rolon-Garrido, M. H. Wagner, C. Luap and T. Schweizer, *J. Rheol.*, 2006, **50**, 327–340.

102 J. K. Nielsen, O. Hassager, H. K. Rasmussen and G. H. McKinley, *J. Rheol.*, 2006, **50**, 453–476.

103 J. E. Glass, *Polymers in Aqueous Media*, American Chemical Society, Washington 1989.

104 F. Meyer, D. Lohmann and W.-M. Kulicke, *J. Rheol.*, 2009, **53**, 799–818.

105 A. O. Bingol, D. Lohmann, K. Puschel and W.-M. Kulicke, *Biorheology*, 2010, **47**, 205–224.

106 D. J. McCarty, in *Arthritis and Allied Conditions. A Textbook of Rheumatology*, ed. D. J. McCarty and W. J. Koopman, Williams and Wilkins, Baltimore, 13 edn, 1997, vol. 1, pp. 81–99.

107 E. A. Balazs, D. Watson, I. F. Duff and S. Roseman, *Arthritis Rheum.*, 1967, **10**, 357–376.

108 G. G. Fuller and L. G. Leal, *Rheologica Acta*, 1980, 19.

109 C. J. Farrell, A. Keller, M. J. Miles and D. P. Pope, *Polymer*, 1980, **21**, 1292–1294.

110 Y. Rabin, *Journal of Polymer Science*, 1985, **23**, 11–13.

111 S. K. Lai, Y.-Y. Wang, D. Wirtz and J. Hanes, *Adv. Drug Delivery Rev.*, 2009, **61**, 86–100.

112 S. P. Carrington, J. A. Odell, L. Fisher, J. Mitchell and L. Hartley, *Polymer*, 1996, **37**, 2871–2875.

113 W.-M. Kulicke, U. Reinhardt, G. G. Fuller and O. Arendt, *Rheol. Acta*, 1999, **38**, 26–33.

114 J. R. Stokes and G. A. Davies, *Biorheology*, 2007, **44**, 141–160.

115 M. Campese, X. Sun, J. A. Bosch, F. G. Oppenheim and E. J. Helmerhorst, *Arch. Oral Biol.*, 2009, **54**, 345–353.

116 G. A. Van Aken, M. H. Vingerhoeds and E. H. A. de Hoog, *Curr. Opin. Colloid Interface Sci.*, 2007, **12**, 251–262.

117 C. L. Hattrup and S. J. Gendler, *Annu. Rev. Physiol.*, 2008, **70**, 431–457.

118 G. H. McKinley and T. Sridhar, *Annu. Rev. Fluid Mech.*, 2002, **34**, 375–415.

119 M. Stelter, G. Brenn, A. L. Yarin, R. P. Singh and F. Durst, *J. Rheol.*, 2002, **46**, 505–527.

120 O. Arnolds, H. Buggisch, D. Sachsenheimer and N. Willenbacher, *Rheol. Acta*, 2010, **49**, 1207–1217.

121 L. Campo-Deano and C. Clasen, *J. Non-Newtonian Fluid Mech.*, 2010, **165**, 1688–1699.

122 M. S. N. Oliveira and G. H. McKinley, *Phys. Fluids*, 2005, **17**, 071704.

123 M. Yao and G. H. McKinley, *J. Non-Newtonian Fluid Mech.*, 1998, **79**, 469–501.

124 S. H. Spiegelberg, D. C. Ables and G. H. McKinley, *J. Non-Newtonian Fluid Mech.*, 1996, **64**, 229–267.

125 V. Sharma, A. Jaishankar, Y.-C. Wang and G. H. McKinley, *Soft Matter*, 2011, **7**, 5150–5160.

126 O. Regev, S. Vandebril, E. Zussman and C. Clasen, *Polymer*, 2010, **51**, 2611–2620.